American Mineralogist, Volume 92, pages 1401–1410, 2007

Microbial effects in promoting the smectite to illite reaction: Role of organic matter intercalated in the interlayer

GENGXIN ZHANG,[1] JINWOOK KIM,[2] HAILIANG DONG,[1,*] AND ANDRE J. SOMMER[3]

[1]Department of Geology, Miami University, Oxford, Ohio 45056, U.S.A.
[2]Naval Research Laboratory, Seafloor Sciences Branch, Stennis Space Center, Mississippi 39529, U.S.A.
[3]Department of Chemistry and Biochemistry, Miami University, Oxford, Ohio 45056, U.S.A.

ABSTRACT

Cysteine and toluene as model organic molecules were intercalated into Fe-rich smectite (nontronite, NAu-2). The illitization of these intercalated smectites as induced by microbial reduction of structural Fe^{3+} was investigated. Iron-reducing bacterium *Shewanella putrefaciens* CN32 was incubated with lactate as the sole electron donor and structural Fe^{3+} in cysteine- and toluene-intercalated NAu-2 (referred to as cysteine-NAu-2 and toluene-NAu-2 hereafter) as the sole electron acceptor. Anthraquinone-2, 6-disulfonate (AQDS) was used as an electron shuttle in bicarbonate buffer. The extent of Fe^{3+} reduction in cysteine-NAu-2 and toluene-NAu-2 was 15.7 and 5.4%, respectively, compared to 20.5% in NAu-2 without organic matter intercalation. In the bioreduced NAu-2, X-ray diffraction, and scanning and transmission electron microscopy did not detect any discrete illite, although illite/smectite mixed layer or high charge smectite phases were observed. In bioreduced cysteine-NAu-2, discrete illite and siderite formed. In contrast, bioreduction of toluene-NAu-2 did not result in any mineralogical changes. The contrasting bioreduction results between cysteine- and toluene-intercalated nontronite may be ascribed to the nature of organic matter-bacteria interactions. Whereas cysteine is an essential amino acid for bacteria and can also serve as an electron shuttle, thus enhancing the extent of Fe^{3+} bioreduction and illitization, toluene is toxic and inhibits Fe^{3+}-reducing activity. This study, therefore, highlights the significant role of organic matter in promoting the smectite to illite reaction under conditions typical of natural environments (i.e., non-growth condition for bacteria).

Keywords: Cysteine, illite, microbial Fe^{3+} reduction, nontronite NAu-2, toluene, *Shewanella putrefaciens* CN32

INTRODUCTION

The smectite-to-illite reaction proceeds through mixed-layer illite-smectite (I-S) intermediates in which the percentage of illite layers increases with increasing temperature (Hower et al. 1976), time (Pytte and Reynolds 1989), K concentration (Huang et al. 1993), and water/rock ratio (Whitney 1990). These empirical relationships have been used to infer paleotemperature and diagenetic grade (Hoffman and Hower 1979). However, ambiguity exists as to the mechanisms by which smectite layers are converted to illite. In one model (Hower et al. 1976), the smectite-to-illite reaction is believed to occur through a sequence of mixed-layer I-S, including smectite-rich R0, R1, R2, R3 I-S (R0 and R1 are Reichwite numbers: R0 = randomly interstratified, R1 = regularly interstratified IS, R2 = IIS, and R3 = ISII), and illite-rich I-S, with a continuously variable ratio in the proportions of smectite and illite layers. The model implies that all I-S with the relative proportions of illite layers from 0 to 100% are likely to occur in nature. This concept led to the implication that the smectite-to-illite transformation can proceed layer-by-layer in the solid state. However, several TEM studies indicated that R1 I-S with 50% illite layers is abundant, whereas other proportions of mixed-layer I-S phases (i.e., R2, R4, etc.) are rarely observed (Ahn and Peacor 1989; Veblen et al. 1990). Using the L.R. White resin (Electron Microscopy Sciences, Hatfield, Pennsylvania) treatment (Kim et al. 1995), Dong et al. (1997) determined that smectite, R1 I-S, and illite are the dominant phases in the I-S series, and that R1 I-S has a unique structure and composition. Recent lattice energy calculations (Stixrude and Peacor 2002) are consistent with that observation. These data (uniqueness of R1 and absence of other mixed layer phases) imply that the smectite to illite reaction occurs via dissolution of smectite and precipitation of illite.

Different mechanisms for the smectite to illite reaction may be in part due to the different conditions of the geological systems studied, including variables such as water/rock ratio, fluid composition, redox state, and presence or absence of organic matter (Dong 2005). Solid-state transformation may be operative in closed systems, where the water/rock ratio is low, whereas dissolution-precipitation may be predominant in open systems, where the water/rock ratio is high. Numerous studies have been performed in support of one model, or the other (Nadeau

* E-mail: dongh@muohio.edu

0003-004X/07/0809–1401$05.00/DOI: 10.2138/am.2007.2331

REPORT DOCUMENTATION PAGE	Form Approved OMB No. 0704-0188

1. REPORT DATE (DD-MM-YYYY)	2. REPORT TYPE	3. DATES COVERED (From - To)
03042007	Journal Article	

4. TITLE AND SUBTITLE

Microbial effects in promoting the smectite to illite reaction: Role of organic matter intercalated in the interlayer

5a. CONTRACT NUMBER

5b. GRANT NUMBER

5c. PROGRAM ELEMENT NUMBER

6. AUTHOR(S)

Gengxin Zhang, JinWook Kim, Hailiang Dong, Andre J. Sommer

5d. PROJECT NUMBER

5e. TASK NUMBER

5f. WORK UNIT NUMBER

7. PERFORMING ORGANIZATION NAME(S) AND ADDRESS(ES)

Naval Research Laboratory
Marine Geoacoustics Division
Stennis Space Center, MS 39529

8. PERFORMING ORGANIZATION REPORT NUMBER

NRL/JA/7430-06-3

9. SPONSORING/MONITORING AGENCY NAME(S) AND ADDRESS(ES)

Office of Naval Research
800 North Quincy Street
Arlington VA 22217-5000

10. SPONSOR/MONITOR'S ACRONYM(S)

ONR

11. SPONSOR/MONITOR'S REPORT NUMBER(S)

12. DISTRIBUTION/AVAILABILITY STATEMENT

Approved for public release; distribution is unlimited

13. SUPPLEMENTARY NOTES

American Mineralogist, Volume 92, pages 1401-1410, 2007

14. ABSTRACT

Cysteine and toluene as model organic molecules were intercalated into Fe-rich smectite (nontronite, NAu-2). The illitization of these intercalated smectites as induced by microbial reduction of structural Fe^{3+} was investigated. Iron-reducing bacterium *Shewanella putrefaciens* CN32 was incubated with lactate as the sole electron donor and structural Fe^{3+} in cysteine- and toluene-intercalated NAu-2 (referred to as cysteine-NAu-2 and toluene-NAu-2 hereafter) as the sole electron acceptor. Anthraquinone-2, 6-disulfonate (AQDS) was used as an electron shuttle in bicarbonate buffer. The extent of Fe^{3+} reduction in cysteine-NAu-2 and toluene-NAu-2 was 15.7 and 5.4%, respectively, compared to 20.5% in NAu-2 without organic matter intercalation. In the bioreduced NAu-2, X-ray diffraction, and scanning and transmission electron microscopy did not detect any discrete illite, although illite/smectite mixed layer or high charge smectite phases were observed. In bioreduced cysteine-NAu-2,

15. SUBJECT TERMS

Cysteine, illite, microbial Fe reduction, nontronite NAu-2, toluene, Shewanella putrefaciens CN32

16. SECURITY CLASSIFICATION OF:			17. LIMITATION OF ABSTRACT	18. NUMBER OF PAGES	19a. NAME OF RESPONSIBLE PERSON
a. REPORT	b. ABSTRACT	c. THIS PAGE			Yoko Furukawa
Unclassified	Unclassified	Unclassified	UU	10	19b. TELEPHONE NUMBER (Include area code) 228-688-5474

et al. 1985; Bethke and Altaner 1986; Eberl and Srodon 1988; Lindgreen and Hansen 1991; Dong and Peacor 1996; Drits et al. 1996; Dong et al. 1997), or both (Whitney and Northrop 1988), but few have taken into account the role of microbes.

Bacteria are ubiquitous in soil and sediments, and have been shown to reduce structural Fe^{3+} in smectite for respiration and growth (Stucki et al. 1987; Gates et al. 1993, 1998; Kostka et al. 1996, 1999a, 1999b; Dong et al. 2003; Kim et al. 2003, 2004). Although it is well established that microbes can reduce Fe^{3+} in the smectite structure, only recently has experimental evidence suggested that microbes may be doing so via a dissolution mechanism (Dong et al. 2003). A recent study (Kim et al. 2004) first demonstrated that microbes can promote the smectite to illite reaction at room temperature within 14 days. Although the extent to which illite was formed from bioreduction of smectite was not quantified in that study, the results are important because this reaction was thought to require a much higher temperature over an extended period of time (Whitney and Northrop 1988; Huang et al. 1993). In abiotic systems, elevated temperatures are typically used in laboratory experiments to accelerate the smectite-to-illite reaction to compensate for a long geological time in nature (e.g., Whitney and Northrop 1988; Bauer and Velde 1999). In biotic systems, bacteria may catalyze the reaction, and elevated temperature or prolonged time may not be necessary.

This paper is an extension of the study by Kim et al. (2004) to further test the hypothesis that bacteria can promote the S-I reaction in presence of other factors such as organic matter. The natural organic matter (amino acids, natural sugar, lignin phenol, etc.) is widely distributed in sediments (Keil et al. 1998) and a significant amount of organic matter is associated with the smectite interlayer (Kennedy et al. 2002). A few previous studies have shown some effects of organic matter in the smectite to illite reaction. For example, Small et al. (1994) demonstrated that potassium oxalate and potassium acetate in neutral-alkaline aqueous solution can significantly promote the smectite to illite reaction. Likewise, abundant illite is observed in organic matter rich black shales relative to sandstones, siltstones, and organic matter poor shales (Uysal et al. 2004). Kostka et al. (1999a) showed that organic acids could promote structural Fe dissolution, a condition conducive to illite formation. Despite these previous studies, it is not yet clear how the presence of organic matter in the smectite interlayer affects microbial Fe^{3+} reduction and the smectite-illite reaction.

The objectives of this study were therefore to understand the role of intercalated organic matter in microbial reduction of Fe^{3+} and the smectite to illite reaction. The present study, therefore, would enhance our fundamental understanding of the S-I reaction in clay-rich sediments and rocks and have significant implications for sediment diagenesis.

MATERIALS AND METHODS

Synthesis of cysteine- and toluene-intercalatronite

Nontronite NAu-2, an Fe-rich variety of smectite from Uley graphite mine, South Australia (the Clay Minerals Society Reference Clay) (Keeling et al. 2000), was used in this study. The formula for this nontronite is $M^{+}_{0.72}(Si_{7.55}Al_{0.45})(Fe_{3.83}Mg_{0.05})O_{20}(OH)_4$, where M may be Ca, Na, or K (Keeling et al. 2000). A clay fraction (0.5–2.0 μm) was separated by centrifugation at 500 g for 12 min to remove quartz, plagioclase, and talc followed by 10 min at 10 000 g to collect nontronite in the suspension. The clay size fraction was then air-dried. The clay sample was then sterilized by a 5 min exposure to microwave radiation (Keller et al. 1988), and sterility was confirmed from lack of bacterial growth in LB broth following a 48 h incubation at 30 °C in the dark under aerobic condition. The total Fe content in NAu-2 is 23.4% (by weight), of which 0.6% is Fe^{2+} (Keeling et al. 2000; Jaisi et al. 2005).

Smectite clays have a large reactive surface area capable of sorbing a large number of dissolved organic compounds (amino acids, natural sugars, lignin phenols, etc.) in natural environments. These clays also make important contributions to pesticide and organic contaminant retention in soils (Sheng et al. 2001; Li et al. 2003, 2004). Among the many different types of organic matter that can possibly be associated with smectite, two particular types were chosen for this study. Cysteine, a type of amino acid, was used as a representative natural organic matter because it is an essential nutrient for many living organisms and can be found in electron-transfer proteins (Doong and Schink 2002). Toluene, a widely distributed carcinogenic hydrocarbon in soils and sediments, was used because a large number of bacteria can degrade it for growth at hydrocarbon-contaminated sites (Rabus et al. 1993; Fries et al. 1994; Alagappan and Cowan 2004).

Cysteine intercalated NAu-2, hereafter called cysteine-NAu-2, was synthesized following a previously published procedure (Brigatti et al. 1999). The first step involves synthesis of homoionic clay. Two grams of nontronite NAu-2 were mixed with 200 mL of 1 *M* $CuCl_2$ solution in a flask, and the suspension was stirred overnight at room temperature. After centrifugation, the supernatant was decanted and replaced by freshly prepared 1 *N* $CuCl_2$ solution. This process was repeated three times. Excess salts were removed from the homoionic clay by dialysis until the aspired solution tested negative with $AgNO_3$. The second step involves cysteine intercalation. Two grams of the homoionic nontronite were suspended in a flask containing 100 mL of 0.05 *M* cysteine solution. The suspension was stirred at room temperature for 24 h. After centrifugation, cysteine-NAu-2 was washed 10 times with distilled water. The amount of cysteine intercalated into NAu-2 was quantified by measuring the difference between the starting and the remaining cysteine concentration in aqueous solution. Cysteine-NAu-2 was stored in airtight tubes until the bioreduction experiments.

Toluene intercalated NAu-2, hereafter called toluene-NAu-2, was synthesized following a published procedure (Sharmasarkar et al. 2000). Hexadecyltrimethylammonium bromide (HDTMA), an organic compound, was purchased from Sigma-Aldrich Company and used to prepare HDTMA-clay suspension. Aqueous solution of HDTMA (20 mg/mL) was added to a clay suspension (10 mg/mL) and it was agitated with a magnetic stirrer. After mixing for 4 h, HDTMA-clay was washed with distilled-deionized water until free of salts and free of aqueous HDTMA. HDTMA intercalated in the interlayer of clay minerals is not toxic to bacteria (Nye et al. 1994; Xu and Boyd 1995). The HDTMA-clay complex of 0.10 g was weighed into a 25-mL centrifuge tube that contained 25 mL of distilled water. A volume of 12 μL toluene/methanol (4.6 μL/7.4 μL) solution was added to the 25 mL tube containing the HDTMA-clay complex, yielding a toluene concentration of 160 mg/L. The tube was shaken for up to 18 h at room temperature. After centrifugation, toluene-NAu-2 was washed 5 times with distilled water. The amount of toluene intercalated into NAu-2 was quantified by measuring the difference between the starting and the remaining toluene concentration in aqueous solution. Toluene-NAu-2 was stored in airtight tubes until use for the bioreduction experiments.

Bacteria and bioreduction experiments

An Fe-reducing bacterium *Shewanella putrefaciens* strain CN32 was routinely cultured aerobically in tryptic soy broth (TSB) (30 g/L) from the stock culture, which was kept at –80 °C. After harvesting in TSB until mid to late log phase, CN32 cells were washed with anaerobic bicarbonate buffer and resuspended in the buffer.

Nontronite NAu-2, cysteine-NAu-2, and toluene-NAu-2 were made into clay slurries (100 mg/mL) in bicarbonate buffer (2.5 g/L $NaHCO_3$, 0.1 g/L KCl). These slurries served as stock solutions for subsequent experiments and were sterilized. In a typical experiment with a 15 mL final volume of culture medium, 1.5 mL of each clay slurry (final concentration, 5 mg/mL) was added to replicate pressure tubes of 23 mL capacity with lactate as the electron donor (20 *mM*) and Fe^{3+} in the nontronite structure as the sole electron acceptor in the presence of an electron shuttling compound anthraquinone-2, 6-disulfonate (AQDS, 0.1 *mM*). Tubes were purged with N_2/CO_2 gas mix (80:20) and sealed with thick butyl rubber stoppers. CN32 cells (1×10^8 and 2×10^8 cells/mL final concentration for cysteine-NAu-2 and toluene-NAu-2 reduction experiments, respectively) were added to the treatment tubes with a sterile and anaerobic syringe. The controls consisted of tubes that received the same amount of sterile bicarbonate buffer in place of CN32 cells. All experiments were incubated at 30 °C with shaking at 60 rpm.

Numeration of cell numbers

Although our experiments were performed under non-growth conditions, nonetheless, cell numbers were numerated at the end of the bioreduction experiments to monitor possible cell death. Cell-clay suspension of 1 mL in volume was removed from the experimental tubes, diluted and plated on agar plates. The number of colony forming units (CFU) was visually counted.

Analyses

Due to the possibility of Fe^{3+} reduction by cysteine during synthesis, Fe^{2+} production was measured by 0.5 *N* HCl extraction. In addition, the total Fe^{3+} and Fe^{2+} contents in cysteine-NAu-2 and toluene-NAu-2 were measured by direct current plasma (DCP) emission spectroscopy and titration (Andrade et al. 2002), respectively.

The extent of microbial reduction of Fe^{3+} in NAu-2 was monitored by measuring Fe^{2+} production. At select time points, 0.5 mL of mineral suspension, sampled with a sterile syringe, was added to a plastic tube pre-added with 0.5 mL of 1 *N* HCl (Ultrex grade, Sigma-Aldrich). The cell-mineral suspension was allowed to stand in HCl for 24 h before analyzing for Fe^{2+}. This extraction is termed the 0.5 *N* HCl extracted Fe^{2+}, and has been shown to be effective for extracting microbially produced Fe^{2+} including adsorbed form and Fe^{2+} in biogenic solids except for highly crystalline magnetite (Fredrickson et al. 1998; Zachara et al. 1998). However, this method only partially extracts structural Fe^{2+}, thus it may slightly underestimate the extent of Fe^{3+} bioreduction (Jaisi et al. 2007).

Aqueous concentration of cysteine during the cysteine-NAu-2 synthesis and the bioreduction experiments was determined by the DTNB method [5,5'-dithiobis(2-nitrobenzoic acid)] (Riddles et al. 1983).Cysteine-NAu-2 suspension (0.2 mL) was centrifuged at 14 000 *g* for 5 min to settle particles. The clear supernatant (0.1 mL) was mixed with 1 *mM* DTNB in 50 *mM* phosphate buffer (pH 8.0). The cysteine concentration was determined with a spectrophotometer at 412 nm. Toluene concentration in aqueous solution was determined by high performance liquid chromatography (HPLC).

X-ray Diffraction

Both nonreduced and bioreduced nontronite, cysteine-NAu-2, and toluene-NAu-2 solid samples were studied by X-ray diffraction (XRD) to identify mineralogical changes as a result of bioreduction. The samples were dried in an anaerobic glove box (95% N_2 and 5% H_2) (Coy Laboratory Products, Grass Lake, Michigan). XRD data were collected with a Scintag X1 powder diffract meter system using Cu*K*α radiation with a variable divergent slit and a solid-state detector. Low-background quartz XRD slides (Gem Dugout, Inc., Pittsburgh, Pennsylvania) were used for the calibration.

Fourier Transform Infrared (FTIR) Spectroscopy

Fourier transform infrared (FTIR) spectroscopy was used to confirm intercalation of cysteine into the interlayer of the nontronite structure and to detect structural changes as a result of bioreduction. Dried clay powder was pressed to form a pellet. Infrared spectra were collected with a Harrick Split-pea ATR microscope interfaced to a Perkin-Elmer 2000 Fourier transform infrared spectrometer. This accessory employed a silicon internal reflection element (IRE) and the standard deuterium triglycine sulfate (DTGS) detector on the Spectrum 2000 macro bench. Spectra collected using this device represent the average of 32 individual scans possessing a spectral resolution of 4 cm^{-1}. The samples were brought into intimate contact with the IRE using a pressure loading of 0.5 kg.

Scanning and transmission electron microscopy (SEM and TEM)

Mineralogical changes were further studied with SEM and TEM. SEM samples were prepared following a previously published procedure (Dong et al. 2003). Briefly, cell-mineral suspensions were fixed in 2.5% glutaraldehyde in bicarbonate solution and one droplet of fixed suspension was placed on the surface of a glass cover slip that was cleaned with 1 mg/mL polylysine solution prior to use. The nontronite particles were allowed to settle onto the cover slip for 15 min. The sample-coated cover slip was sequentially dehydrated using varying proportions of ethanol and distilled water followed by critical point drying to preserve delicate biological texture. The cover slip was mounted onto a SEM stub and Au coated for observation using a Zeiss Supra 35 FEG-VP SEM. The SEM was operated at an accelerating voltage of 10 to 15 kV. A short working distance (6–10 mm) and low beam current (30–40 mA) were used to achieve the best image resolution. A longer working distance (8 mm) and higher beam current (50–70 mA) were used for qualitative energy dispersive spectroscopy (EDS) analysis.

Both nonreduced control and bioreduced solid samples were imbedded with Nanoplast resin and sliced using a microtome for TEM observations (Kim et al. 2003, 2004). The advantage of using hydrophilic Nanoplast resin in this study is that solvent exchange (methanol/water exchange) is not required, which is necessary in the L.R. White resin impregnation technique (Kim et al. 1995). Because solvent exchange can cause artifacts, such as dissolution of organic matter, this Nanoplast resin is preferred. High magnification (up to 400 000 times) was applied for measurements of secondary mineral phases to resolve fine lattice fringes. A JEOL 3010 TEM operating at 300 keV with a LaB_6 filament was used for all TEM analyses. Sample preparations for TEM and SEM observations were performed in an anaerobic glove box except during critical point drying, Au coating, polymerization of resin, and microtoming.

Results

Characterization of cysteine- and toluene-intercalated nontronites

The amount of cysteine absorbed into nontronite was 92 mg per gram of NAu-2. Most of the cysteine was incorporated into the interlayer of the nontronite structure. Because cysteine is a reductant, even though the synthesis of cysteine-NAu-2 was carried out in air, there was 28.4% of Fe^{3+} reduction. This Fe^{3+} reduction could mostly likely have happened after dissolved oxygen in the aqueous solution was consumed by cysteine, as it is an effective oxygen scavenger (Logan et al. 2005). When oxidized by oxygen, cysteine converts into cystine. Thus, some amount of cysteine may have been lost via this pathway and the cysteine concentration in cysteine-NAu-2 (92 mg/g) may be overestimated.

As a result of Fe^{3+} reduction and its subsequent solubilization during the synthesis, the total Fe content in cysteine-NAu-2 decreased to 15.1% (relative to the weight of Cu cysteine-NAu-2), and 0.01% of which was Fe^{2+}. The total Fe content was 18% relative to the weight of the original NAu-2. The sum of this remaining Fe^{3+} in cysteine-NAu-2 and that released into aqueous solution was the same as that originally present in NAu-2. This solubilization may have some impacts on the NAu-2 structure, although such changes were not detected by XRD, FTIR, SEM, and TEM.

The increase in the d_{001} spacing from 11.08 Å (at $2\theta = 7.96°$) for nontronite NAu-2 to 18.8 Å (at $2\theta = 4.7°$) for cysteine-NAu-2 confirms that cysteine was intercalated into the interlayer of the nontronite structure (NAu-2) (Fig. 1a). The IR spectrum for cysteine-NAu-2 shows changes of main functional groups relative to native NAu-2 (Fig. 2). In particular, the characteristic absorption bands of NH_3^+ (3130–3030 and 1640–1610 cm^{-1}), COO^- (1600–1650 cm^{-1}), and CH_2 (2926–2853 cm^{-1}) indicates that the interlayer cysteine formed complex with the interlayer Cu^{2+} in the nontronite structure (Brigatti et al. 1999).

The amount of toluene intercalated into the interlayer of the nontronite structure per gram of NAu-2 was 43 mg. The total Fe content in toluene-NAu-2 was 20.0%, only slightly lower than 23.4% for NAu-2. The Fe^{2+} content was 0.74% of the total Fe. Rather than any loss of Fe during synthesis, this decrease in the total Fe content was most likely caused by an increase of the weight of nontronite due to addition of HDTMA and toluene in the interlayer. The d_{001} spacing of toluene-NAu-2 increased to 14.02 Å after HDTMA and toluene were intercalated into the

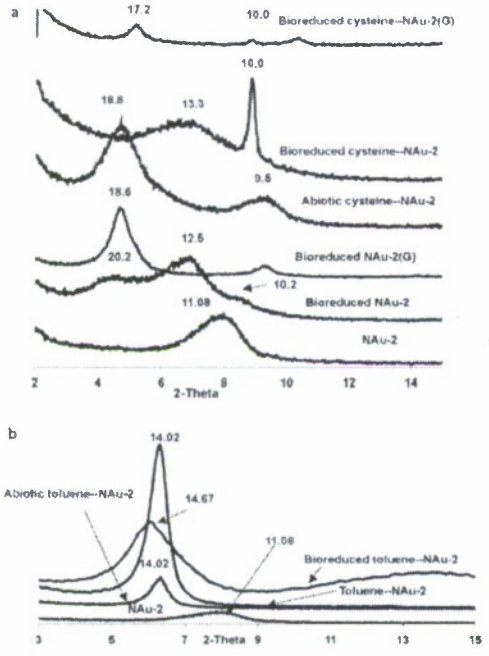

nontronite structure (Fig. 1b). The d_{001} layer spacing of 14.02 Å appears to be low for NAu-2 (Keeling et al. 2000). Yaron-Marcovich et al. (2005) observed the layer spacing of 16 to 19 Å for HDTMA-intercalated montmorillonite (Swy-1), with the layer spacing depending on the specific loading of HDTMA and thus different mechanisms of its interactions with expandable clay mineral. It is possible that the layer spacing may be as low as 14.02 Å when the loading of HDTMA is lower than 60%.

Microbial reduction of Fe^{3+} in nontronite and organic matter intercalated nontronite

The extent of Fe^{3+} bioreduction in NAu-2 reached 20.5% (or 0.86 mmol per gram of NAu-2) in 41 days (Fig. 3a), similar to that observed previously in our laboratory (Jaisi et al. 2005). During the same time period, 15.7% (0.42 mmol/g) of Fe^{3+}

◀FIGURE 1. (a) XRD patterns for oriented specimens of NAu-2, bioreduced NAu-2, ethylene glycolated bioreduced NAu-2, abiotic cysteine-NAu-2 control (no cells added), bioreduced cysteine-NAu-2, and ethylene glycolated, bioreduced cysteine-NAu-2. (b) XRD patterns for oriented specimens of NAu-2, toluene-NAu-2, and abiotic toluene-NAu-2 control (no cells added), and bioreduced toluene-NAu-2(G): sample was solvated with ethylene glycol vapor at 65 °C. Cysteine-NAu-2 denotes NAu-2 with intercalated cysteine in the interlayer. Toluene-NAu-2 denotes NAu-2 with intercalated toluene in the interlayer.

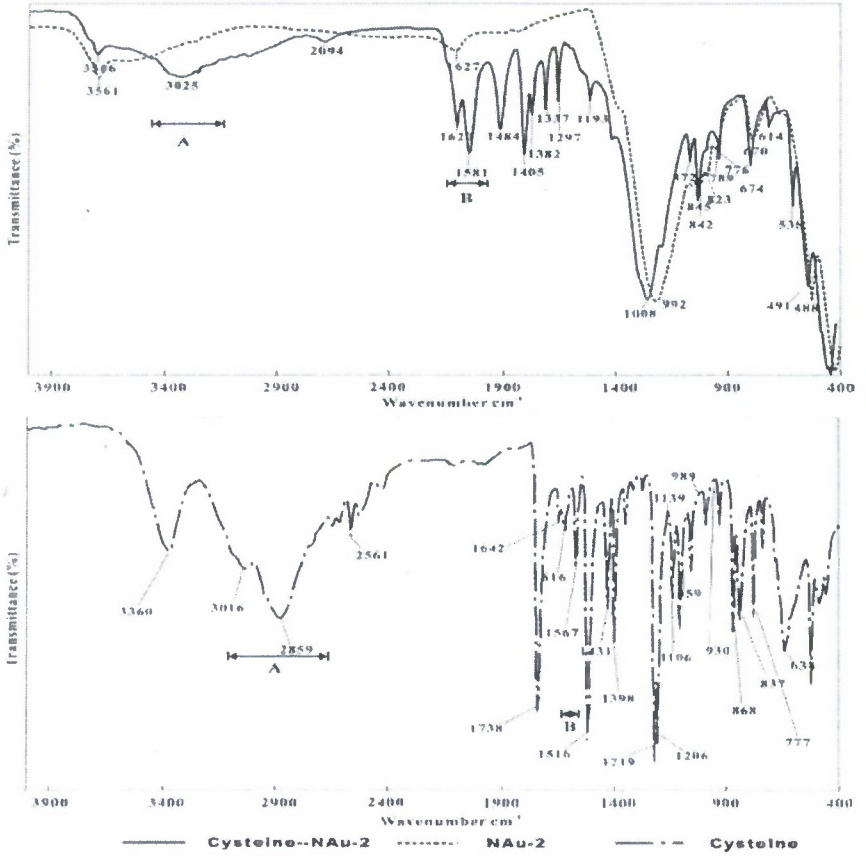

FIGURE 2. Comparison of FTIR spectra for nontronite, cysteine, and cysteine-NAu-2 complex. Label A refers to the stretching of CH_2 (2926–2853 cm^{-1}) and NH^{3+} groups (3130–3030); label B refers to NH^{3+} deformation and COO^- asymmetric stretching modes.

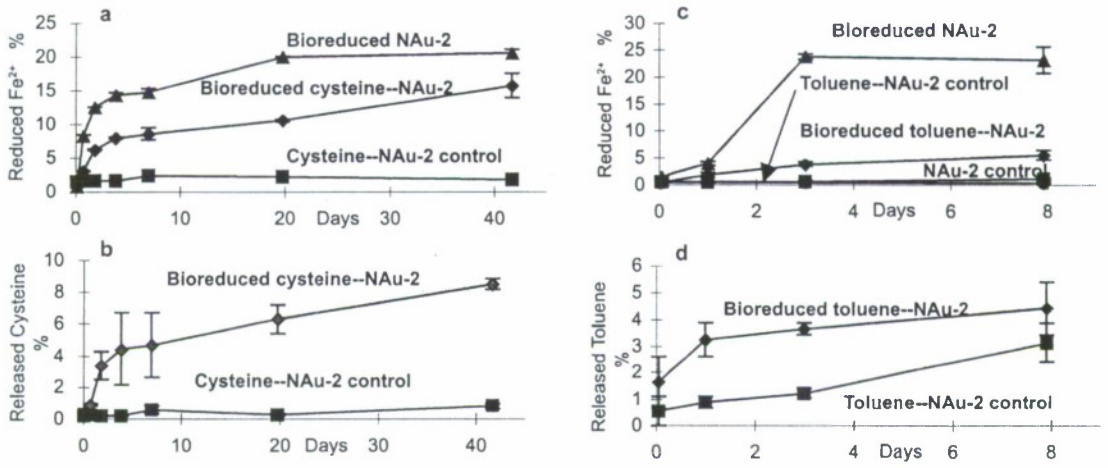

FIGURE 3. (**a**) Fe^{3+} reduction with time as measured by 0.5 *M* HCl-extractable Fe^{2+} in bioreduced NAu-2, cystiene-NAu-2, and cystiene-NAu-2 control (no cells added). (**b**) Release of cysteine into aqueous solution from the cysteine-NAu-2 complex as a result of bioreduction. (c) Fe^{3+} reduction with time as measured by 0.5 *M* HCl-extractable Fe^{2+} in NAu-2 control (no cells), bioreduced NAu-2, toluene-NAu-2, and toluene-NAu-2 control (no cells added). (**d**) Release of toluene into aqueous solution from toluene-NAu-2 complex as a result of bioreduction and in the control (no cells added). All results were from duplicate treatments.

bioreduction was measured for cysteine-NAu-2 (relative to the amount of Fe^{3+} remaining in this complex). Over the course of the bioreduction, 8.5% of cysteine was slowly released into aqueous solution while no cysteine was released in the control (Fig. 3b), suggesting partial dissolution of cysteine-NAu-2 upon Fe^{3+} reduction. Because the relative partitioning of the released cysteine between clay surfaces and aqueous solution was not known, it was not possible to determine the mass balance of the interlayer cysteine as a result of bioreduction.

In contrast to the bioreduction of Fe^{3+} in cysteine-NAu-2, the extent of Fe^{3+} bioreduction in toluene-NAu-2 was only 5.4% (0.20 mmol/g) in 8 days (Fig. 3c), and 4.4% of toluene was released into solution (Fig. 3d). There was little difference in the amount of toluene release between the abiotic control and bioreduced toluene-NAu-2.

Cell numeration

The viable cell number was counted to be 2.2×10^6 cells/mL in the bioreduced cysteine-NAu-2 sample and only 4.5×10^5 cells/mL in the bioreduced nontronite. These cell numbers represented a significant decrease from the initial concentration of 1×10^8 cells/mL, but this decrease was less for the bioreduced cysteine-NAu-2 system than for the nontronite system. In the toluene-NAu-2 experiment, the cell number was 5×10^5 and 2.1×10^7 in the bioreduced toluene-NAu-2 and the bioreduced NAu-2, respectively. These cell numbers again represented a significant decrease from the initial concentration, but this decrease was more for the toluene-NAu-2 system than NAu-2 alone.

X-ray diffraction

The structural changes of nontronite NAu-2 and cysteine-NAu-2 upon microbial Fe^{3+} reduction were detected by XRD (Fig. 1). Bioreduction of Fe^{3+} in nontronite resulted in disappearance of the peak at 11.08 Å ($2\theta = 7.96°$) and appearance of peaks at 12.5 Å ($2\theta = 7.1°$), 20.1 Å ($2\theta = 4.4°$), and 10.2 Å ($2\theta = 8.6°$). The peaks for cysteine-NAu-2 at $2\theta = 4.7$ and 9.4°, which corresponded to $d_{001} = 18.8$ Å and $d_{002} = 9.5$ Å, respectively, disappeared upon Fe^{3+} reduction. Instead, two new peaks at $2\theta = 6.8$ and 8.9° with d-spacings of 13.3 and 10.0 Å, respectively, appeared in the bioreduced cysteine-NAu-2. These two new peaks more likely corresponded to high charge nontronite (Gates et al. 1998) and discrete illite (Kim et al. 2004), respectively. To confirm that the 10 Å peak was from discrete illite, the bioreduced material was treated with ethylene glycol. The 10 Å illite peak remained at the same position and two new peaks 17.2 and 8.6 Å, the first- and second-order of expanded smectite peak, appeared at the expense of the 13.3 Å peak. The observed broadening and reduced intensity of the illite peaks might have been caused by a small amount of material on the glass slide, thin illite particles, and possible inter-particle diffraction. The d_{001} spacing of the bioreduced toluene-NAu-2 slightly increased from 14 to 14.6 Å, and that of the abiotic control remained at 14 Å (Fig. 1b).

Scanning electron microscopy

Irregular flaky particles were observed in the abiotic cysteine-NAu-2 control with scanning electron microscopy (SEM) (Fig. 4a). Qualitative SEM energy dispersive spectroscopy (EDS) showed a very low Al/Si ratio, typical of the starting NAu-2 composition. The relatively low Fe content was caused by loss of a large fraction of Fe during synthesis of this material. A high amount of C, S, and Cu was probably due to the interlayer cysteine-Cu^{2+} complex (inset in Fig. 4a). Particles in the bioreduced cysteine-NAu-2, however, were more rounded than those in the control (Fig. 4b). In addition, new mineral precipitates (labeled as A, B, C, D, and E) were observed with different chemical compositions (the inset in Fig. 4b). The elemental composition of grain A exhibited a high Al/Si ratio, low Fe, and high K content, typical of illite. Grain B was identified as biogenic silica. Grain C was identified as residual cysteine-intercalated NAu-2. Grain D showed a significant amount of increase in the Al con-

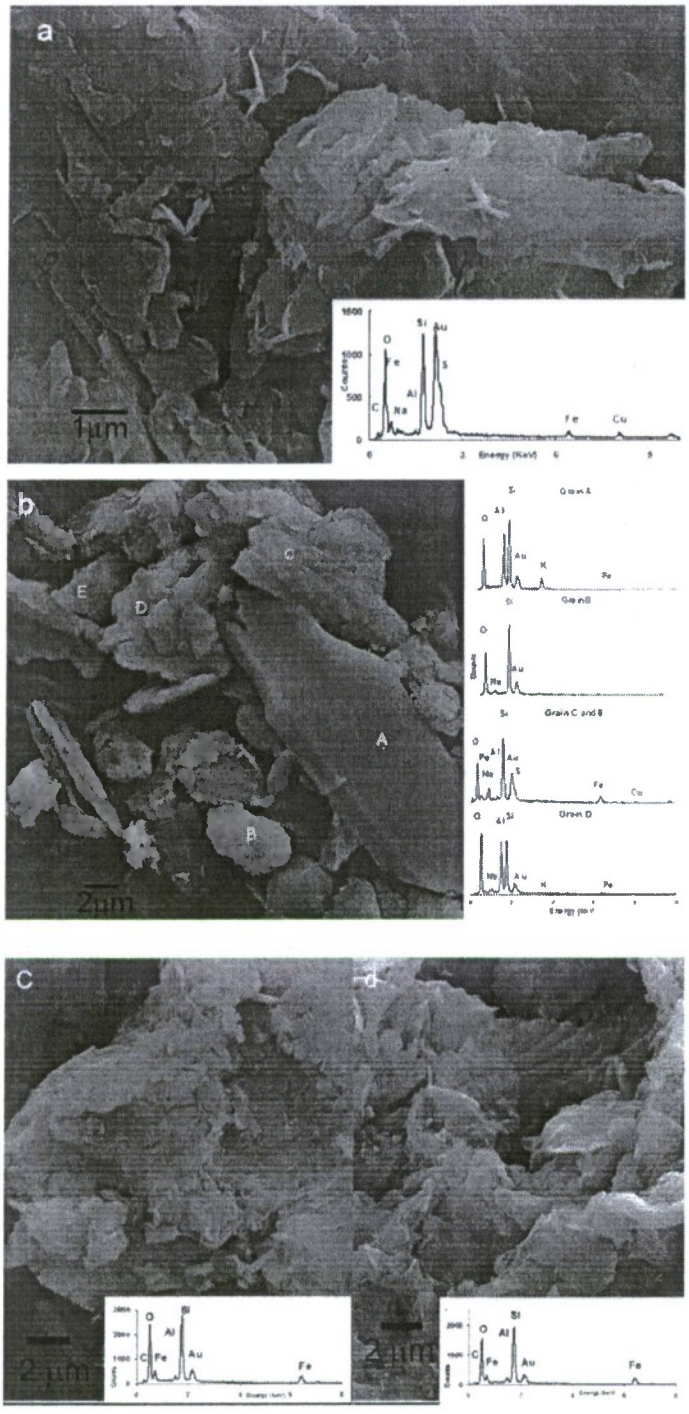

FIGURE 4. (a) Secondary electron image showing the remaining cysteine-NAu-2 complex in the abiotic control after 41 days of incubation. The inset is a SEM-EDS spectrum of the cysteine-NAu-2 complex showing a typical elemental composition of the complex. The Au peak is from Au coating, and the Cu peak is from the interlayer. (b) Secondary electron image showing bioreduced cysteine-NAu-2 after 41 days of incubation. The right panel shows SEM-EDS spectra of Grains A, B, C, D, and E. The absence of the Cu peak in these spectra may indicate that these materials are different from the starting cysteine-NAu-2 and may represent newly precipitated materials. (c) Secondary electron image showing the remaining toluene-NAu-2 complex in the abiotic control (no added cells) after 8 days of incubation. The inset is a SEM-EDS spectrum of toluene-NAu-2 complex showing a typical elemental composition. (d) Secondary electron image showing bioreduced toluene-NAu-2 after 8 days of incubation. The inset is a SEM-EDS spectrum of bioreduced toluene-NAu-2 showing no change in the composition.

tent (relative to grain C and E) and a low amount of K content. High C, S, and Cu contents, which were detected in the control (Fig. 4a), disappeared in grain D and E. Grain D and E might be newly precipitated intermediate phases between nontronite and illite, such as high charge nontronite. Bioreduced toluene-NAu-2 and its control were also characterized with SEM. No obvious changes were observed in either morphology or element composition (Figs. 4c and 4d).

Transmission electron microscopy (TEM)

Lattice fringe spacings were measured for a total of 56 and 124 packets for bioreduced and nonreduced cysteine-NAu-2,

respectively. Layer spacings of 14 and 15 Å were dominant in the unreduced cysteine-NAu-2 (Figs. 5 and 6a). The difference in the d_{001} spacing between XRD and TEM measurements was most likely caused by some extent of dehydration under high vacuum in the electron column of TEM. The Fe^{3+} bioreduction decreased the proportions of larger layer spacings (14 and 15 Å) and increased smaller ones (10 to 12 Å) (Fig. 5). A mixture of Fe-rich precipitates, newly formed illite phases (I), and residual cysteine-NAu-2 packets (12–13 Å layer spacings) were observed in the bioreduced sample (Fig. 6b). Illite was identified based on the EDS composition (the inset of Fig. 6b) showing a high Al/Si ratio and K content. The high Fe content was most likely due to contamination of illite by the Fe-rich precipitates. The inset selected area electron diffraction (SAED) of the Fe-precipitates (outlined area in Fig. 6b) displayed the ring patterns with 1.9, 2.8, and 3.5 Å spacings (Fig. 6c). These layer spacings were consistent with siderite. High magnification (up to 400 K times) TEM was employed to capture the structure of secondary phase minerals (Fig. 7). Aggregates of the Fe-precipitates mixed with 11 Å spacings of clay layers were dominant (Fig. 7a). The outlined area in Fig. 7a, when magnified, showed randomly oriented nanoparticles with the dominant spacings of 3.6 Å (Fig. 7b). The particle size of the Fe precipitates was small, often less than 30–60 Å. The inset SAED pattern showed three strongest rings, with d-spacings of 3.6, 2.7, and 2.9 Å, respectively. These spacings were consistent with siderite. The newly formed illite

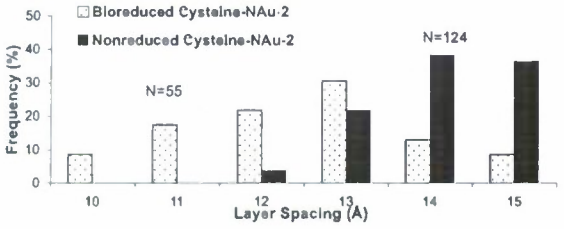

FIGURE 5. A histogram showing the distribution of layer spacings in the cysteine-NAu-2 complex as a result of bioreduction in comparison with the abiotic control (no cells added). Total 56 and 124 packets for bioreduced and nonreduced cysteine-NAu-2 were measured.

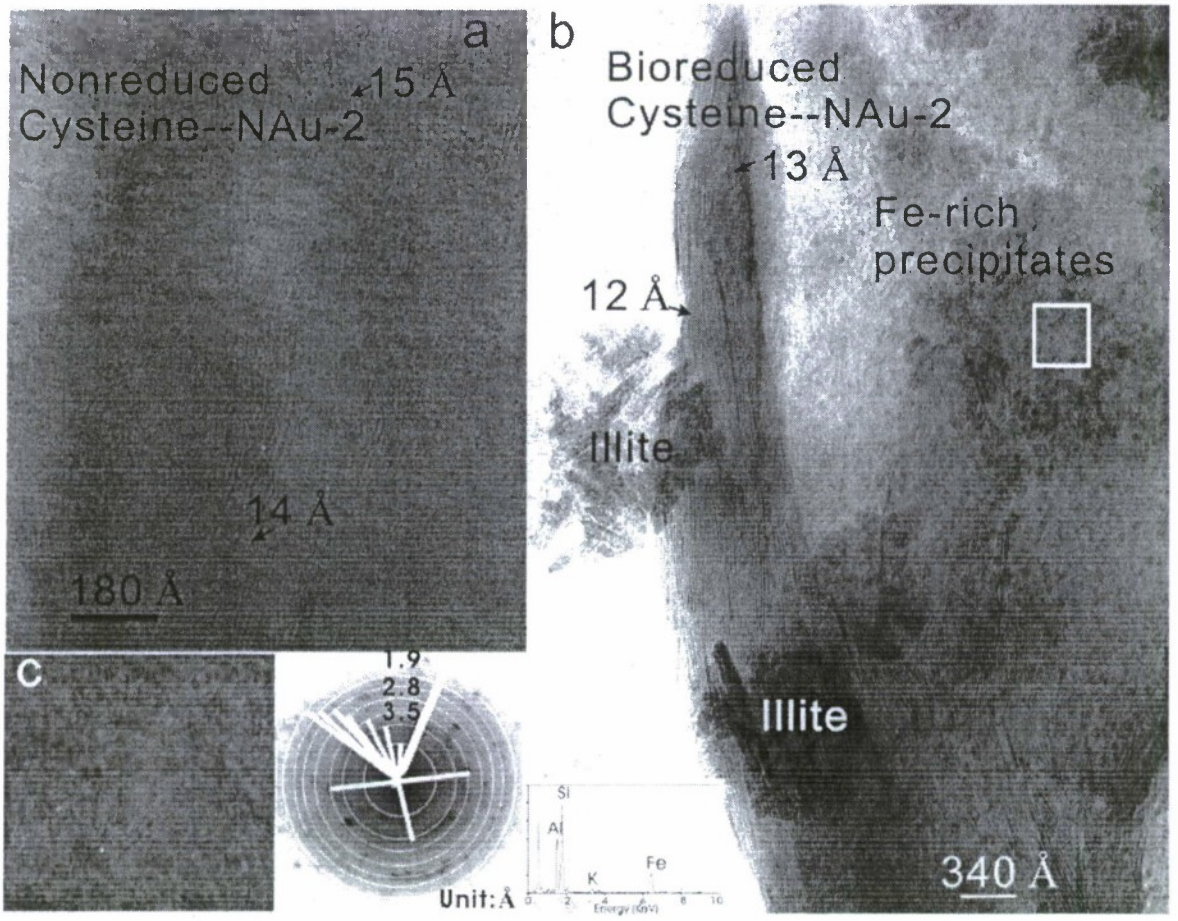

FIGURE 6. TEM micrographs of (a) nonreduced cysteine-NA-2 with layer spacings of 14–15 Å; (b) bioreduced cysteine-NAu-2 showing Fe-precipitates and illite (I) particles. The inset EDX shows typical illite composition of high Al/Si ratio and K; (c) high magnification image of the outlined area in b showing randomly oriented fringes with 1.9, 2.8, and 3.5 Å spacings on the SAED pattern, typical of siderite.

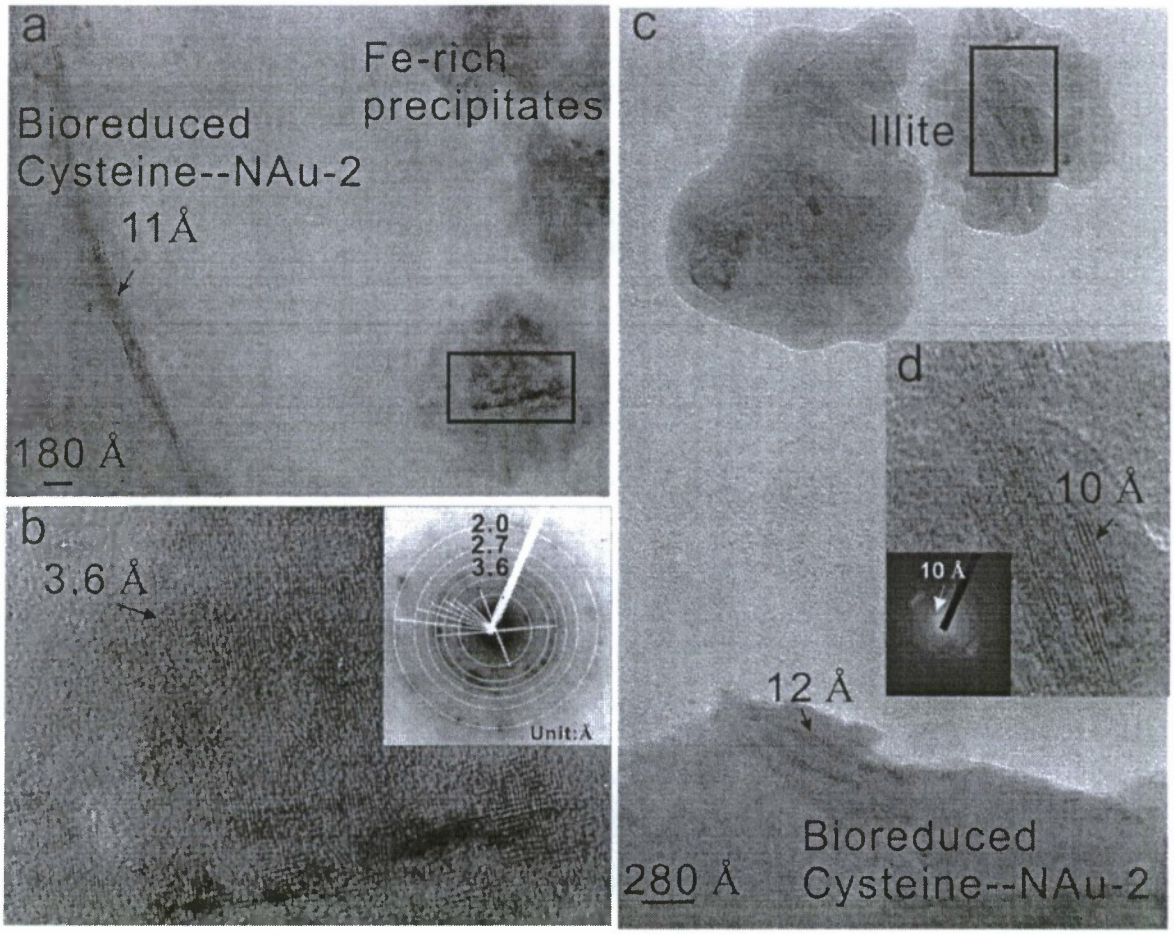

FIGURE 7. TEM micrographs of (a) bioreduced cysteine-NAu-2 with 11 Å layers and Fe-precipitate mixtures; (b) high magnification of the outlined area showing 3.6 Å fringes and typical siderite diffraction patterns with strong diffractions of 2.0, 2.7, and 3.6 Å spacings; (c) illite precipitates having 10 Å lattice fringes confirmed with SAED pattern.

aggregates (I) with residual cysteine-NAu-2 (12 Å spacings) were displayed in Fig. 7c. The outlined area of the aggregates in Figure 7c, when magnified, showed an illite packet consisting of 8–10 layers with 10 Å spacings (Fig. 7d). The inset SAED pattern displayed the diserete Bragg reflections of illite with d_{001} = 1.0 nm. In contrast to the extensive mineralogical changes that occurred in the cysteine-NAu-2, the d_{001} layer spacings of toluene-NAu-2 did not change and the biogenic minerals were not preeipitated as a result of bioreduetion (Figs. 8a and 8b). Total 76 and 97 packets for nonreduced and bioreduced toluene-NAu-2 were measured on the lattice fringes and the average value of layer spacing for both was 14 Å.

DISCUSSION

Influence of interlayer organie matter on Fe^{3+} bioreduction

The two types of organie matter present in the interlayer of the nontronite structure exhibited a contrasting behavior in influencing Fe^{3+} bioreduction. The extent of Fe^{3+} reduction for cysteine-NAu-2 and NAu-2 was similar within 41 days, despite the lower amount of Fe^{3+} in cysteine-NAu-2. In contrast, the presence of toluene signifieantly decreased the extent of Fe^{3+} bioreduction relative to pure NAu-2.

Cysteine, when present in aqueous solution, can serve as an eleetron shuttle or mediator, thus signifieantly stimulating the reduction extent of Fe^{3+} in cultures of *Geobacter sulfurreducens* (Doong and Schink 2002). In our experiments, the cysteine released into aqueous solution could have served as an electron shuttle, thus enhancing Fe^{3+} bioreduction. However, an external electron shuttle, AQDS, was already present in the system. Thus, the presence of an additional electron shuttle may not have had mueh effect as shown in our data (Fig. 3a). Cysteine is also a known essential amino acid for bacteria and its presence may have promoted cell growth and Fe^{3+} bioreduction. Indeed, in comparison with the extent of decrease in cell number in the bioreduction experiment with NAu-2 alone (from 1×10^8 to 4.5×10^5 cells/mL), this decrease was mueh less for the cysteine-NAu-2 system (from 1×10^8 to 2.2×10^6 cells/mL).

In contrast, toluene is not a nutrient and may even be toxie. Thus its presenee may inhibit bacterial activity (Stiner and Hal-

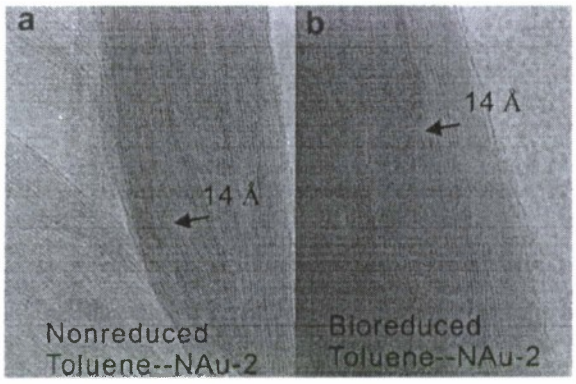

FIGURE 8. TEM micrographs of (a) nonreduced and (b) bioreduced toluene-NAu-2 lattice fringes. 14 Å layer spacings were dominant for both samples.

verson 2002). So the presence of toluene, even in a solid matrix, may have inactivated CN32 cells and may have been responsible for the decreased extent of Fe^{3+} bioreduction relative to that with nontronite alone (without toluene). Indeed, our data showed a significant decrease in cell number (from 2×10^8 to 5×10^5 cells/mL) in the presence of toluene relative to the bioreduction of nontronite alone (from 2×10^8 to 2.1×10^7 cells/mL).

Promotion of the smectite to illite reaction by organic matter

Our data conclusively showed that certain types of organic matter, when intercalated in the interlayer of the smectite structure, facilitated illitization via reductive dissolution of nontronite. Cysteine could have multiple effects on promoting the smectite to illite reaction. It is an essential nutrient for bacterial growth. So its presence, even in the interlayer of the nontronite structure, would have been attractive to CN32 cells. They may have attacked it by dissolving the nontronite structure, thus resulting in an enhanced extent of Fe^{3+} bioreduction (Fig. 3a) and release of the intercalated cysteine into aqueous solution (Fig. 3b). The released cysteine, as an organic acid, would have a catalytic effect on the smectite illitization, similar to the effects of potassium oxalate and potassium acetate on this reaction (Small 1994).

This study supplements our previous study in that microbes play an important role in promoting the smectite to illite reaction (Kim et al. 2004). This reaction typically requires conditions of 300 to 350 °C, 100 MPa, and 4–5 months in the absence of microbial activity. But in its presence, it takes place at 1 atmosphere and room temperature. In our early study, a growth medium was used, where the smectite to illite reaction may have been coupled with microbial growth. In our current study, we have demonstrated that even in a non-growth medium, more typical of natural environments, this microbially mediated reaction can take place, as long as there is cysteine present in the interlayer of the nontronite structure. Cysteine is a natural degradation product of organic matter and may be present in soils and sediments. Thus, cysteine, nontronite, and Fe-reducing microorganisms may co-exist in natural environments and may be important in promoting the smectite to illite reaction, even when microbial growth conditions are absent. In our laboratory study, the source of K for illite formation was the bicarbonate buffer, but in nature, K-rich fluids and K-bearing minerals may serve as important sources.

The presence of toluene in the interlayer of the nontronite structure significantly inhibited Fe^{3+} bioreduction of nontronite, even in the presence of an electron shuttle AQDS. As a result, there was no nontronite dissolution and illite formation. These data suggest that toluene may be toxic to CN32 cells, and its presence may have inactivated CN32 reducing activity. Alternatively, the presence of toluene in the interlayer may have partially blocked the electron transfer chain, thus making Fe^{3+} bioreduction more difficult. Because of the presence of toluene, AQDS could not even enter the interlayer to facilitate the electron transfer.

Stability of Cu-cysteine complex in natural environments

A previous study (Brigatti et al. 1999) has shown that Cu-cysteine complex within the interlayer of the smectite structure is stable and can be resistant to migration in soils and ground waters. Thus, Cu, as a toxic heavy metal, may be sequestered via this mechanism (Brigatti et al. 1999). The results of this study, however, point out the importance of understanding the effect of microorganisms on metal sequestration into clay minerals. If the smectite contains a certain amount of Fe^{3+} in the structure, and if Fe-reducing bacteria are present, these bacteria can reduce the structural Fe^{3+} under anoxic conditions, partially dissolve the clay structure, and thus remobilize Cu. Iron-reducing bacteria are abundant in soils and sediments (Lovley 2000). Recently, even thermophilic Fe-reducing bacteria have been found in the subsurface (Boone et al. 1995; Kashefi and Lovley 2003; Roh et al. 2002), highlighting the importance of understanding biogeochemistry in designing metal sequestration technologies.

ACKNOWLEDGMENTS

This research was supported by a grant from National Science Foundation (EAR-0345307). Some part of this research was supported by a student grant from the Clay Mineral Society (Student Research Grant 2004) to G.Z. J.W.K. publishes with NRL contribution number NRL/JA/7430-06-3. We are grateful to Joseph Stucki and an anonymous reviewer for their constructive comments.

REFERENCES CITED

Ahn, J.H. and Peacor, D.R. (1989) Illite/smectite from Gulf Coast: a reappraisal of transmission electron microscope images. Clays and Clay Minerals, 37, 542–546.

Alagappan, G. and Cowan, R.M. (2004) Effect of temperature and dissolved oxygen on the growth kinetics of Pseudomonas putida F1 growing on benzene and toluene. Chemosphere, 54(8), 1255–1265.

Andrade, S., Hypolito, R., Ulbrich, H.H.G.J., and Silva, M.L. (2002) Iron(II) oxide determination in rocks and minerals. Chemical Geology, 182, 85–89.

Bauer, A. and Velde, B. (1999) Smectite transformation in high molar KOH solutions. Clay Minerals, 34(2), 259–273.

Bethke, C.M. and Altaner, S.P. (1986) Layer-by-layer mechanism of smectite illitization and application to a new rate law. Clays and Clay Minerals, 34, 136–145.

Boone, D.R., Liu, Y., Zhao, Z., Balkwill, D.L., Drake, G.R., Stevens, T.O., and Aldrich, H.C. (1995) *Bacillus infernus sp. nov.*, an Fe^{3+}- and Mn(IV)-reducing anaerobe from the deep terrestrial subsurface. International Journal of Systematic Bacteriology, 45(3), 441–448.

Brigatti, M.F., Lugli, C., Montorsi, S., and Poppi, L. (1999) Effects of exchange cations and layer-charge location on cysteine retention by smectites. Clays and Clay Minerals, 47(5), 664–671.

Dong, H. (2005) Interstratified Illite-smectite: A review of contributions of TEM data to crystal chemical relation and reaction mechanisms. Clay Science, 12(supplement 1), 6–12.

Dong, H. and Peacor, D.R. (1996) TEM observations of coherent stacking relations in smectite, I/S and illite of shales: evidence for MacEwan crystallites and

dominance of $2M_1$ polytypism. Clays and Clay Minerals, 44, 257–275.
Dong, H., Peacor, D.R., and Freed, R.L. (1997) Phase relations among smectite, R1 I/S and illite. American Mineralogist, 82, 379–391.
Dong, H., Kostka, J.E., and Kim, J.W. (2003) Microscopic evidence for microbial dissolution of smectite. Clays and Clay Minerals, 51(5), 502–512.
Doong, R.A. and Schink, B. (2002) Cysteine-mediated reductive dissolution of poorly crystalline iron(III) Oxides by "Geobacter sulfurreducens." Environmental Science and Technology, 36(13), 2939–2945.
Drits, V.A., Salyn, A.L., and Sucha, V. (1996) Structural transformations of interstratified illite-smectites from Dolna Ves hydrothermal deposits: dynamics and mechanisms. Clays and Clay Minerals, 44, 181–190.
Eberl, D.D. and Srodon, J. (1988) Oswald ripening and interparticle-diffraction effects for illite crystals. American Mineralogist, 73, 1335–1345.
Fredrickson, J.K., Zachara, J.M., Kennedy, D.W., Dong, H.L., Onstott, T.C., Hinman, N.W., and Li, S.M. (1998) Biogenic iron mineralization accompanying the dissimilatory reduction of hydrous ferric oxide by a groundwater bacterium. Geochimica et Cosmochimica Acta, 62(19–20), 3239–3257.
Fries, M.R., Zhou, J., Chee-Sanford, J., and Tiedje, J.M. (1994) Isolation, characterization, and distribution of denitrifying toluene degraders from a variety of habitats. Applied and Environmental Microbiology, 60, 2802–2810.
Gates, W.P., Wilkinson, H.T., and Stucki, J.W. (1993) Swelling Properties of Microbially Reduced Ferruginous Smectite. Clays and Clay Minerals, 41(3), 360–364.
Gates, W.P., Jaunet, A.M., Tessier, D., Cole, M.A., Wilkinson, H.T., and Stucki, J.W. (1998) Swelling and texture of iron-bearing smectites reduced by bacteria. Clays and Clay Minerals, 46(5), 487–497.
Hoffman, J. and Hower, J. (1979) Clay mineral assemblages as low grade metamorphic geothermometers: application to the thrust-faulted disturbed belt of Montana, U.S.A. In P.A. Scholle and P.R. Schluger, Eds., Aspects of diagenesis, 26, p. 55–80. Society of Economic Paleontologists and Mineralogists Special Publication, Tulsa, Oklahoma.
Hower, J., Eslinger, E.V., Hower, M.H., and Perry, E.A. (1976) Mechanism of burial metamorphism of argillaceous sediments. 1. Mineralogical and chemical evidence. Geological Society of America Bulletin, 87, 725–737.
Huang, W.-L., Longo, J.M., and Pevear, D.R. (1993) An experimentally derived kinetic model for smectite-to-illite conversion and its use as a geothermometer. Clays and Clay Minerals, 41, 162–177.
Jaisi, D.P., Kukkadapu, R.K., Eberl, D.D., and Dong, H.L. (2005) Control of Fe^{3+} site occupancy on the rate and extent of microbial reduction of Fe^{3+} in nontronite. Geochimica et Cosmochimica Acta, 69(23), 5429–5440.
Jaisi, D.P., Dong, H., and Liu, C. (2007) Influence of biogenic Fe(II) on the extent of microbial reduction of Fe(III) in clay mineral nontronite, illite, and chlorite. Geochimica et Cosmochimica Acta, 71, 1145–1158.
Kashefi, K. and Lovley, D.R. (2003) Extending the upper temperature limit for life. Science, 301, 934.
Keeling, J.L., Raven, M.D., and Gates, W.P. (2000) Geology and characterization of two hydrothermal nontronites from weathered metamorphic rocks at the Uley Graphite Mine, South Australia. Clays and Clay Minerals, 48(5), 537–548.
Keil, R.G., Tsamakis, E., Giddings, J.C., and Hedges, J.I. (1998) Biochemical distributions (amino acids, neutral sugars, and lignin phenols) among size-classes of modern marine sediments from the Washington coast. Geochimica et Cosmochimica Acta, 62(8), 1347–1364.
Keller, M.D., Bellows, W.K., and Guillard, R.R.L. (1988) Microwave Treatment for sterilization of phytoplankton culture media. Journal of Experimental Marine Biology and Ecology, 117(3), 279–283.
Kennedy, M.J., Pevear, D.R., and Hill, R.J. (2002) Mineral surface control of organic carbon in black shale. Science, 295(5555), 657–660.
Kim, J.W., Peacor, D.R., Tessier, D., and Elsass, F. (1995) A technique for maintaining texture and permanent expansion of smectite interlayers for TEM observations. Clays and Clay Minerals, 43, 51–57.
Kim, J.W., Newell, S., Furukawa, Y., Lavoie, D., and Daulton, T. (2003) Characterization of microbially Fe^{3+}-reduced nontronite: environmental cell transmission electron microscopy. Clays and Clay Minerals, 51(4), 382–389.
Kim, J.W., Dong, H., Seabaugh, J., Newell, S.W., and Eberl, D.D. (2004) Role of microbes in the smectite-to-illite reaction. Science, 303(5659), 830–832.
Kostka, J.E., Stucki, J.W., Nealson, K.H., and Wu, J. (1996) Reduction of structural Fe^{3+} in smectite by a pure culture of *Shewanella putrefaciens* strain MR-1. Clays and Clay Minerals, 44(4), 522–529.
Kostka, J.E., Haefele, E., Viehweger, R., and Stucki, J.W. (1999a) Respiration and dissolution of iron(III)-containing clay minerals by bacteria. Environmental Science and Technology, 33, 3127–3133.
Kostka, J.E., Wu, J., Nealson, K.H., and Stucki, J.W. (1999b) The impact of structural Fe^{3+} reduction by bacteria on the surface chemistry of smectite clay minerals. Geochimica et Cosmochimica Acta, 63(22), 3705–3713.
Li, H., Sheng, G.Y., Teppen, B.J., Johnston, C.T., and Boyd, S.A. (2003) Sorption and desorption of pesticides by clay minerals and humic acid-clay complexes. Soil Science Society of America Journal, 67(1), 122–131.
Li, H., Teppen, B.J., Laird, D.A., Johnston, C.T., and Boyd, S.A. (2004) Geochemical modulation of pesticide sorption on smectite clay. Environmental Science and Technology, 38(20), 5393–5399.
Lindgreen, H. and Hansen, P.L. (1991) Ordering of illite/smectite in Upper Jurassic claystones from the North Sea. Clay Minerals, 26, 105–125.
Logan, B.E., Murano, C., Scott, K., Gray, N.D., and Head, I.M. (2005) Electricity generation from cysteine in a microbial fuel cell. Water Research, 39(5), 942–952.
Lovley, D.R. (2000) Fe^{3+} and Mn(IV) reduction. In D.R. Lovley, Ed., Environmental microbe-metal interactions, p. 3–30. ASM Press, Washington, D.C.
Nadeau, P.H., Wilson, M.J., McHardy, W.J., and Tait, J.M. (1985) The conversion of smectite to illite during diagenesis: evidence from some illitic clays from bentonites and sandstones. Mineralogical Magzine, 49, 393–400.
Nye, J.V., Guerin, W.F., and Boyd, S.A. (1994) Heterotrophic activity of microorganisms in soils treated with quaternary ammonium-compounds. Environmental Science and Technology, 28, 944–951.
Pytte, A.M. and Reynolds, R.C., Jr. (1989) The thermal transformation of smectite to illite. In N.D. Naeser, and T.H. McCulloh, Eds., Thermal history of sedimentary basins: Methods and case histories, p. 133–140. Springer-Verlag, New York.
Rabus, R., Nordhaus, R., Ludwig, W., and Widdel, F. (1993) Complete oxidation of toluene under strictly anoxic conditions by a new sulfate-reducing bacterium. Applied and Environmental Microbiology, 59, 1444–1451.
Riddles, P.W., Blakeley, R.L., and Zerner, B. (1983) Reassessment of Ellman Reagent. Methods in Enzymology, 91, 49–60.
Roh, Y., Liu, S.V., Li, G.S., Huang, H.S., Phelps, T.J., and Zhou, J.Z. (2002) Isolation and characterization of metal-reducing Thermoanaerobacter strains from deep subsurface environments of the Piceance Basin, Colorado. Applied and Environmental Microbiology, 68(12), 6013–6020.
Sharmasarkar, S., Jaynes, W.F., and Vance, G.F. (2000) BTEX sorption by montmorillonite organo-clays: TMPA, ADAM, HDTMA. Water Air and Soil Pollution, 119(1–4), 257–273.
Sheng, G.Y., Johnston, C.T., Teppen, B.J., and Boyd, S.A. (2001) Potential contributions of smectite clays and organic matter to pesticide retention in soils. Journal of Agricultural and Food Chemistry, 49(6), 2899–2907.
Small, J.S. (1994) Fluid composition, mineralogy and morphological-changes associated with the smectite-to-illite reaction—an experimental investigation of the effect of organic-acid anions. Clay Minerals, 29(4), 539–554.
Stiner, L. and Halverson, L.J. (2002) Development and characterization of a green fluorescent protein-based bacterial biosensor for bioavailable toluene and related compounds. Applied and Environmental Microbiology, 68(4), 1962–1971.
Stixrude, L. and Peacor, D.R. (2002) First-principles study of illite-smectite and implications for clay mineral systems. Nature, 420, 165–168.
Stucki, J.W., Komadel, P., and Wilkinson, H.T. (1987) Microbial reduction of structural iron(III) in smectites. Soil Science Society of America Journal, 51(6), 1663–1665.
Uysal, I.T., Glikson, M., Golding, S.D., and Southgate, P.N. (2004) Hydrothermal control on organic matter alteration and illite precipitation, Mt Isa Basin, Australia. Geofluids, 4, 131–142.
Veblen, D.R., Guthrie, G.D., Livi, K.J.T., and Reynolds, R.C., Jr. (1990) High-resolution transmission electron microscopy and electron diffraction of mixed-layer illite/smectite: experimental results. Clays and Clay Minerals, 38, 1–13.
Whitney, G. (1990) Role of water in the smectite to illite reaction. Clays and Clay Minerals, 38, 343–350.
Whitney, G. and Northrop, H.R. (1988) Experimental investigation of the smectite to illite reaction: dual reaction mechanisms and oxygen-isotope systematics. American Mineralogist, 73, 77–90.
Xu, S. and Boyd, S.A. (1995) Cationic surfactant sorption to a vermiculitic subsoil via hydrophobic bonding. Environmental Science and Technology, 29, 312–320.
Yaron-Marcovich, D., Chen, Y., Nir, S., and Prost, R. (2005) High resolution electron microscopy structural studies of organo-clay nanocomposites. Environmental Science and Technology, 39, 1231–1238.
Zachara, J.M., Fredrickson, J.K., Li, S.M., Kennedy, D.W., Smith, S.C., and Gassman, P.L. (1998) Bacterial reduction of crystalline Fe^{3+} oxides in single phase suspensions and subsurface materials. American Mineralogist, 83, 1426–1443.

MANUSCRIPT RECEIVED MAY 28, 2006
MANUSCRIPT ACCEPTED APRIL 3, 2007
MANUSCRIPT HANDLED BY WARREN HUFF